



## Sulfur Removal from Iraqi Kerosene by Oxidative Desulfurization Using Cobalt Molybdate/Graphene Composite

Omar .G. Hammoodi<sup>1\*</sup>, Emaad.T.Bakir Al-Tikrity<sup>1</sup>, Karim. H. Hassan<sup>2</sup>

<sup>1</sup> College of science/ University of Tikrit, Tikrit, Iraq.

<sup>2</sup> College of science/ University of Diyala, Baqubah, Diyala, Iraq.

### ABSTRACT

In this study, a nanocomposite cobalt molybdate/Graphene was prepared by the precipitation method. CoMoO<sub>4</sub>/G nanocomposite was identified by (FTIR,XRD,AFM, and SEM). The composite CoMoO<sub>4</sub>/G was used to remove sulfur from the Iraqi kerosene obtained from the refinery of the Dora. Oxidative desulfurization was used in the sulfur removal of kerosene, and the composite appeared to have good effectiveness in the removal of sulfur from this kerosene under various conditions (Time, temperature, O/S ratio, and catalyst weight) as it showed a high removal rate of sulfur at optimum conditions which exceeded 93%.

**Keywords:** Oxidative desulfurization, Kerosene, Composite, Cobalt molybdate, Sulfur removal.

**Corresponding author:** Omar .G. Hammoodi

**e-mail** ✉ [omarghazih@gmail.com](mailto:omarghazih@gmail.com)

**Received:** 19 November 2018

**Accepted:** 27 March 2019

### 1. INTRODUCTION

Since exhaust gases containing SO<sub>x</sub> have been one of the major sources of air pollution and acid rain, much attention has been focused on the deep desulfurization of light oils (Yazu et al., 2001; Babich and Moulijn, 2003). The organic sulfur-containing compounds in fuels produce toxic sulfur oxide gases by the combustion, which can cause adverse effects on the environment (Lei, et al., 2016). Mercaptans as a kind of sulfur compounds have been undesirable because of their foul odors and corrosive properties (Kumar et al., 201). Therefore, the desulfurization of fuels is extremely important to environmental safety that has become a main challenge of the world. To achieve this purpose, global sulfur levels would be limited to less than 15 ppm in the near future (Triantafyllidis and Deliyanni, 2014). The conventional sulfur compound removing method has been catalytic hydro desulfurization (HDS), which requires both a high temperature and high pressure of hydrogen gas to produce fuel having low levels of sulfur compounds. Nevertheless, the efficiency of HDS has been limited to treat benzothiophenes (BTs) and dibenzothiophenes (DBTs) (Ma, Sakanishi and Mochida, 1994; Kabe, Ishihara and Tajima, 1992). As an alternative technology, an oxidative desulfurization (ODS) process that operates under moderate conditions without requiring H<sub>2</sub> has been extensively investigated (De Filippis and Scarsella, 2003; Bösmann et al., 2001; Hulea, Fajula and Bousquet, 2001; Zhao et al., 2007; Te, Fairbridge and Ring, 2001; Deshpande, Bassi and Prakash, 2005; Otsuki et al., 2000). Since Oxidative desulfurization (ODS) can be applied under mild conditions, like relatively low temperature, pressure and cost of operation comparing with HDS, it has been regarded as an optimum method for deep

desulfurization technology (Babich and Moulijn, 2003; Breyse et al., 2003; Gui et al., 2010).

### 2. EXPERIMENTAL DETAILS:

#### 2.1. Material used:

Graphite Powder (99% purity) was purchased from OMA Company, potassium permanganate, sodium nitrate, sulfuric acid (98%), hydrogen peroxide (30%), hydrazine hydrate, cobalt nitrate hexahydrate, sodium molybdate, Dibenzothiophene, kerosene, ethanol and distilled water. were analytical grade and were used without any purification. The kerosene used were obtained from Dora refinery in Baghdad with specifications given in below table:

**Table 1.** Specifications of kerosene used in the current study

Test	Result
Density 15 °C	0.7906 g/cm <sup>3</sup>
Flash point (Adel) °C	47.4
Final Boiling point °C	245
Doctor Test	Neg.
Distilled 185 °C Vol %	25
Sulfur Content Wt. %	0.0020
Smoke point (mm)	28
Aromatics Content Vol. %	13
Calorific Value Kcal/Kg (gross)	11087

#### 2.2. Preparation of nanomaterials:

##### 2.2.1. Preparation of graphene oxide and Graphene:

Hummer method (William, Hummers and Offeman, 1958) was used to oxidize the graphite for the synthesis of GO as follows: 2 gm of graphite, 1.3gm of sodium nitrate and 50 ml of sulfuric acid were placed in a 500 ml reaction flask, and then immersed in ice bath. They were then mixed and stirred at 0 °C for 15 minutes. Then, 6gm of potassium permanganate was added

slowly to the above solution and cooled for 30 minutes. The suspended solution was stirred continuously for 1 hour at 35°C, and 92 ml water was added drop wise to the suspension for 10 minutes. The solution was left stirring for 1hr. Subsequently, the suspension was diluted by 280 ml of warm water and stirred for 4 hours and maintained at room temperature, treated with 15 ml (30%) H<sub>2</sub>O<sub>2</sub> to reduce the residual permanganate to soluble manganese ions. Finally, the resulted suspension was filtered, washed with distilled water, and dried in a vacuum oven at 70°C for 24 hours to obtain GO. Graphene was synthesized in a typical procedure as follows, GO (100 mg) was loaded in a 250 ml round bottomed flask, and (50 ml) water was then added, yielding a homogeneous yellow-brown dispersion solution. This was sonicated until it became clear with no visible particulate matter. Hydrazine hydrate (1.00 ml) was then added, and the solution was heated in an oil bath at 100°C using a water-cooled condenser for 24h. The reduced black solid GO gradually precipitated out. This product was isolated by filtration, and then washed continuously five times with 100 ml of distilled water, and finally dried in an oven at 70°C for 24 hours.

### 2.2.2. Preparation of cobalt molybdate and cobalt molybdate/Graphene:

To prepare the hybrid CoMoO<sub>4</sub>/nano composites, the microwave-assisted one-pot synthesis was developed. In a typical procedure, 1 mmol of Co(NO<sub>3</sub>)<sub>2</sub>·6H<sub>2</sub>O was dissolved in 20 ml deionized water, then 20 ml deionized water containing 1 mmol of Na<sub>2</sub>MoO<sub>4</sub>·2H<sub>2</sub>O was added dropwise and stirred for 2 h to form a pink suspension. Subsequently, 1 ml of NH<sub>4</sub>OH (25%) was added to the mixture. The obtained mixture was put in the center of a house-hold microwave oven (800 W), and irradiated for 5 min, and then the oven was turned off and the mixture rested for 2 min, after that, the oven was turned on again to irradiate the mixture for another 5 min. for collecting the finally produced mixture, it was filtrated, then washed several times with deionized water and absolute ethanol; respectively, and then dried in a vacuum oven at 80 °C for 12 h and calcinated in furnace at 600°C (Rudge et al., 1994). To disperse CoMoO<sub>4</sub> nanoparticles on G, CoMoO<sub>4</sub>, G was dispersed into absolute ethanol, and ultrasonically treated for 10 min. The obtained mixture was dried at 60°C for 10 hr in the oven, and then ethanol was vaporized, leaving behind CoMoO<sub>4</sub> nanoparticles well anchored on G. By changing the amount of CoMoO<sub>4</sub>, several samples with G content of 5%,10% and 15% were prepared.

### 2.2.3. Oxidative desulfurization process:

The kerosene sample with a sulfur concentration of 500 ppm was prepared from hydrotreated kerosene which contained 20 ppm of sulfur and DBT by mixing the required amounts, then the oil bath was first heated up and stabilized at 60°C. 20 cm<sup>3</sup> of thus prepared kerosene, H<sub>2</sub>O<sub>2</sub> oxidant (O/S = 5) and composite (0.4g) were put into the round-bottom flask, and refluxed at the atmospheric pressure with vigorous stirring (900 rpm) for 0.75 hour. After that, the oxidized kerosene was extracted by DMF, (DMF to Kerosene ratio of 1 to 6), and followed by the separation of kerosene from DMF in a separating funnel (Mokhtar et al., 2015).

The percentage of the removal of sulfur compounds was calculated by applying the following equation:

$$Y = \frac{(C_o - C_t)}{C_o} * 100$$

Where C<sub>o</sub> = initial concentration of total sulfur in the Kerosene, C<sub>t</sub> = total sulfur concentration in the treated Kerosene after the reaction for (t) minutes.

## 3. RESULTS AND DISCUSSION:

### 3.1. Characterization of nanocomposites:

#### 3.1.1. FTIR analysis:

##### 3.1.1.1. FTIR of graphene oxide:

The FTIR spectrum of GO in figure 1a, shows a broad band at 3429.5 cm<sup>-1</sup> of -OH in the high frequency region. The band of stretching (C=O) appeared at 1723.8 cm<sup>-1</sup>. While the band centered at 1625 cm<sup>-1</sup> assigned to (C=C) bonds associated with skeletal vibrations of unoxidized graphite domains, 1416 cm<sup>-1</sup> represented the vibrations of (C-O) of carboxylic acid. Finally, the absorption bands at 1230 cm<sup>-1</sup> and 1054.6 cm<sup>-1</sup> were corresponding to the stretching vibrations of C-O of epoxy and alkoxy groups. The stretching vibrations at 1054.6 cm<sup>-1</sup> on the GO and reduced GO spectra indicated the presence of (C-C) skeletal vibrations of the graphite ring.

##### 3.1.1.2. FTIR of graphene:

After the GO was chemically reduced, the intensities of the FTIR peaks corresponding to the oxygen-containing functionalities decreased significantly, especially the peak at 3429 cm<sup>-1</sup> of the -OH vibration. This result indicated that the majority of the oxygen-containing functionalities in GO have been successfully removed by the reduction process, which was consistent with the XRD result. The stretching vibrations at 1083.8 cm<sup>-1</sup> on the reduced GO spectra indicated the presence of (C-C) skeletal vibrations of the graphite ring. However, new bands corresponding to (C=C) stretching, vibration at 1562.9 and 1394.7 cm<sup>-1</sup> were observed representing the bond (C=C) in the graphene ring structure; which indicated that the reduction results were in the formation of sp<sup>2</sup> carbon structure (Silverstin, 1962). Figure 1b shows the FTIR of reduced graphene oxide.

##### 3.1.1.3. FTIR of cobalt molybdate nanoparticle:

Figure 1c shows the FTIR spectra of CoMoO<sub>4</sub> in which the spectra revealed the presence of three major bands at 945.45, 625.45, and 407.27 cm<sup>-1</sup>. The band observed at 945.45cm<sup>-1</sup> corresponded to the vibrational modes of distorted MoO<sub>4</sub> present in CoMoO<sub>4</sub>, and the band at 625.45 cm<sup>-1</sup> corresponded to the vibrational mode of Mo-O in the CoMoO<sub>4</sub>, and the one at 407.27 cm<sup>-1</sup> represented the vibrations due to the Co and Mo building blocks of CoMoO<sub>4</sub> (Nakamoto, 1997; Kianpour, Salavati-Niasari and Emadi, 2013).

##### 3.1.1.4. FTIR of cobalt molybdate-reduced graphene oxide:

Figure 1d shows the FTIR spectrum of CoMoO<sub>4</sub>-G powders. The broad peak centered at 3436 cm<sup>-1</sup> owed to the hydroxyl (O-H) stretching mode. It was revealed that peaks centered at 944.87 and 864 cm<sup>-1</sup> ascribed to the symmetric and asymmetric stretching vibration of O-Mo-O. However, a peak located at 663.3 cm<sup>-1</sup> was ascribed to Co-Mo-O stretching vibration (Sieber et al., 1983).

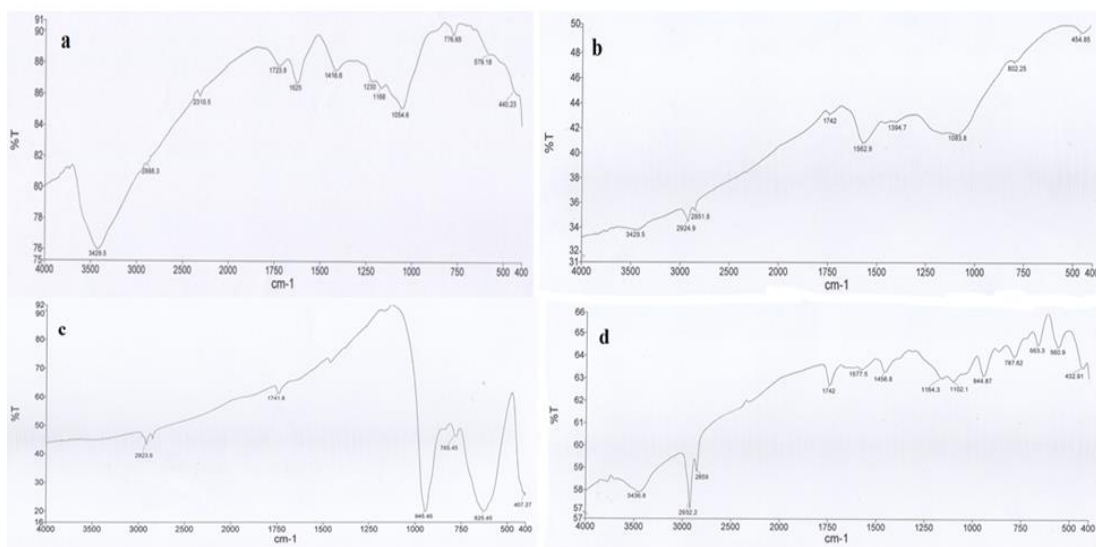


Figure 1. FTIR spectra of (a) GO, (b) G, (c) CoMoO<sub>4</sub>, and (d) CoMoO<sub>4</sub>-G

### 3.1.2. X-Ray Diffraction Characterization (XRD):

The structures of the various modified samples were investigated by X-ray diffraction.

#### 3.1.2.1. X-Ray diffraction of Graphene Oxide:

Figure 2a shows the X-ray diffraction pattern (XRD) of GO powder. The disappearance of a sharp peak near ( $2\theta = 26.49^\circ$ ) (002) showed the changing in the crystalline structure of the graphite, and indicated the destroying the crystalline form of graphite. A large interlayer spacing was created equal to  $8.803\text{Å}$  at the position of ( $2\theta = 10.0392^\circ$ ) (001), and the other two bands at ( $2\theta = 25.9346^\circ$ ) were attributed to the intermediate, beside the peak at ( $2\theta = 54.3^\circ$ ).

#### 3.1.2.2. X-ray Diffraction of graphene:

From the XRD pattern of graphene, in figure 2b, the major broad peak was observed at about ( $2\theta = 26.49^\circ$ ) (002). This gave an interlayer spacing of approximately  $3.54\text{ Å}$ . This interlayer spacing was much smaller than the  $8.803\text{Å}$  for GO, and was closer to the graphite peak. Additionally, it had a broad shoulder at approximately ( $2\theta = 43^\circ$ ) (100). The disappearing of the major strong peak at ( $2\theta = 10.0392^\circ$ ) in graphene indicated that the graphene oxide was converted to graphene.

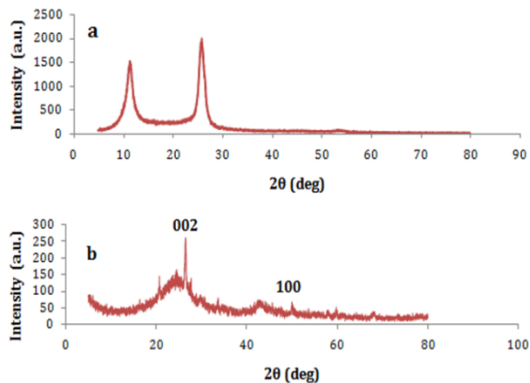


Figure 2. XRD of (a) GO and (b) G.

#### 3.1.2.3. X-ray Diffraction of cobalt molybdate:

The crystalline nature of the chemically prepared CoMoO<sub>4</sub> was examined by XRD; the results have been shown in figure 3a. The sharp diffraction peak at  $26.5058$  corresponded to the reflections of the (002) plane. The other diffraction peaks at  $13.2035$ ,  $19.0702$ ,  $23.3281$ ,  $25.5015$ ,  $27.2492$ ,  $29.0622$ ,  $32.9513$ ,  $33.7046$ ,  $36.7580$ ,  $38.8696$ ,  $40.2263$ ,  $45.1381$ ,  $47.0191$ ,  $52.0682$ , and  $54.5455$  could be assigned to the reflections of the (001), (-201), (021), (201), (-112), (310), (022), (-222), (400), (040), (003), (113), (421), (-204), and (440) planes; respectively. The observed diffraction peaks were in good agreement with the standard patterns for monoclinic CoMoO<sub>4</sub> (JCPDS card no. 00-021-0868). Moreover, there were no peaks due to the impurities or other residuals, indicating the high purity of the chemically synthesized CoMoO<sub>4</sub> nanostructures.

#### 3.1.2.4. X-ray Diffraction of cobalt molybdate-graphene:

The XRD patterns for the as-prepared materials were presented in figure 3b. The main diffraction peaks at  $2\theta$  of  $27.5^\circ$ ,  $33.7^\circ$ ,  $58.4^\circ$  in CoMoO<sub>4</sub>-G were attributed to the (-2 0 2), (-2 2 2), (0 2 4) lattice planes; respectively, which were consistent with the CoMoO<sub>4</sub> (JCPDS, card No. 00.021-0868). The weak and wide diffraction peaks at  $2\theta$  of  $26.5058^\circ$  in G were corresponding to the lattice plane of (0 0 2). The results implied the formation of a carbon framework with relatively higher degree of graphitization. The (0 0 2) diffraction peak became lightly weaker and wider in CoMoO<sub>4</sub>-G, this meant that the degree of crystallization of the G decreased due to the incorporation of CoMoO<sub>4</sub>.

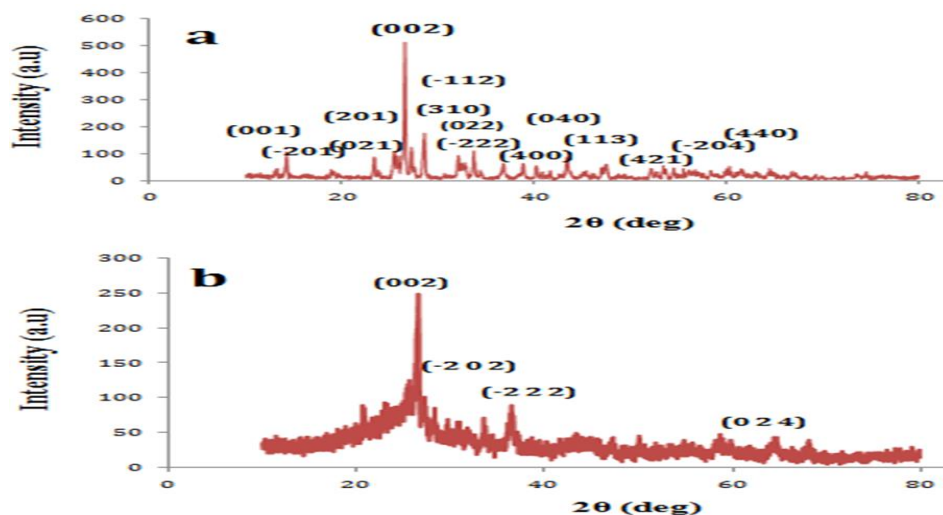


Figure 3. XRD of (a) CoMoO<sub>4</sub> and (b) CoMoO<sub>4</sub>-G.

**3.1.3. AFM of nanocomposites:**

**3.1.3.1. AFM of graphene oxide:**

The AFM image shown in figure 4a represents the graphene oxide produced by Hydro thermal method. It was clear that this method produced GO sheets exfoliated from graphite, overlapping each other despite the separation from each other, and this was confirmed by the process of imaging force microscopy. Measurements of AFM indicated that the highest thickness of the sheets was 21.03 nm in the three dimensional forms of the sample. The length of the sheet was 2361.55 nm. The height of the sheet was examined (13.10 nm). Such sheet

thickness value has been suggested to indicate the presence of oxidized functional groups on the sides of single GO sheets. The graphene oxide was prepared in nano size.

**3.1.3.2. AFM of graphene:**

The AFM measurement showed the graphene sheets with thickness about 8.88nm. With the exception the sheets which doped with oxide CoMoO<sub>4</sub>, and the image of measurement indicated that the graphene sheets were produced by reducing the functional groups on sides of single GO sheets. Figure 4b illustrates the reduced graphene oxide.

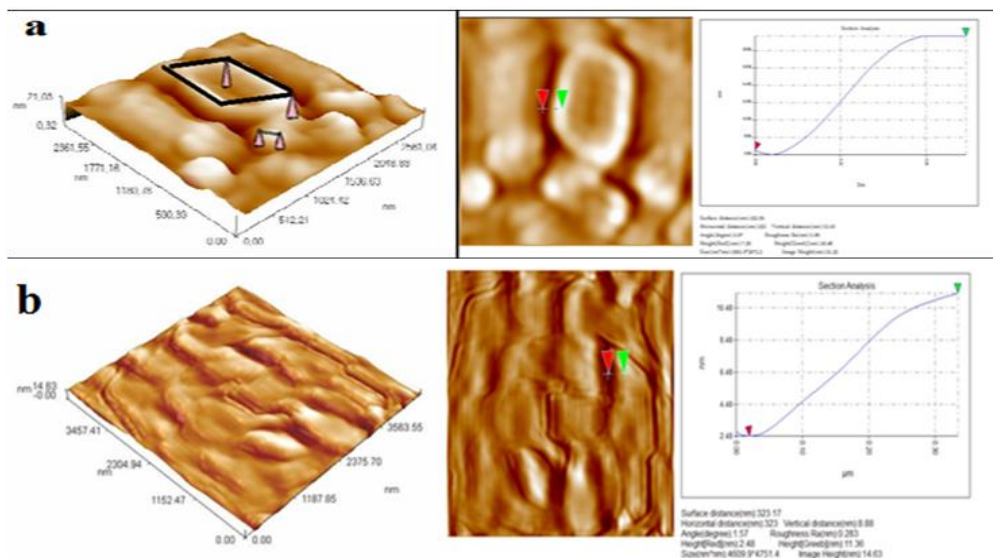


Figure 4. AFM of (a) GO and (b) G.

**3.1.3.3. AFM of Cobalt molybdate**

Figure 5 representing the AFM image of CoMoO<sub>4</sub> shows the particle size distribution of 10% of diameter: 40.00 nm, 50% of diameter: 60.00 nm, and 90% of diameter: 90.00 nm with finally the average diameter equal to 65 nm; and the height of detected place was 21.66nm.

**3.1.3.4. AFM of Cobalt Molybdate- graphene:**

The AFM image shown in figure 6 indicated that the thickness of the CoMoO<sub>4</sub>-G was about 10.13nm, while the height and length of the CoMoO<sub>4</sub>-G were 10.13nm, and 159nm; respectively, the measurements of AFM showed that CoMoO<sub>4</sub> nanoparticles covered the graphene sheets.

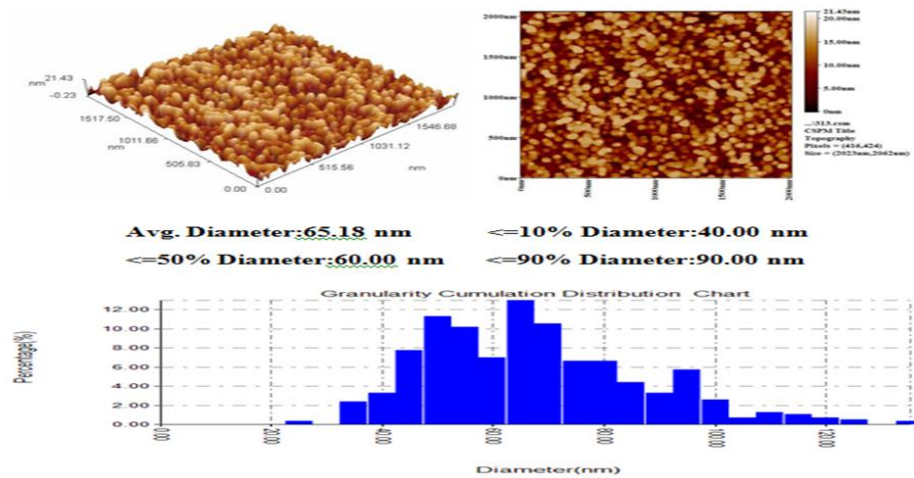


Figure 5. AFM CoMoO<sub>4</sub>.

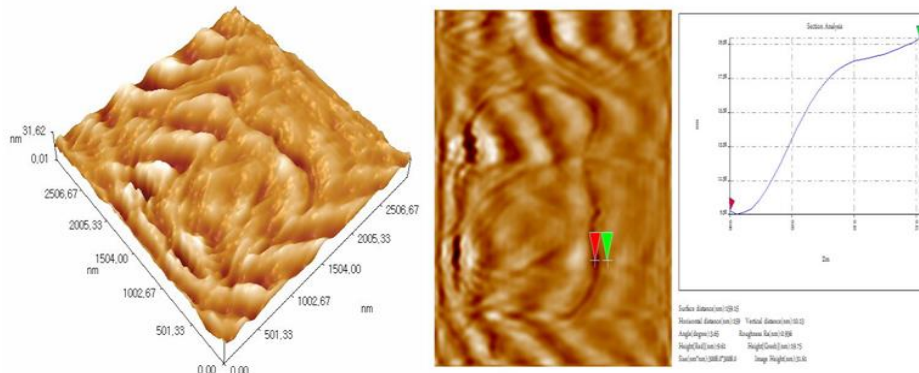


Figure 6. AFM of CoMoO<sub>4</sub>-G

**3.1.4. Scanning Electron Microscope:**

**3.1.4.1. SEM of graphene:**

The scanning electron microscopy of the reduced graphene oxide showed that the G was in the form of sheets, but there were some abnormalities in this sheet due to the oxidation and reduction of the graphite, and this was fully consistent with atomic force microscopy assays, seen in figure 7a.

**3.1.4.2. SEM of cobalt molybdate:**

Figure 7b shows the scanning electron microscopy of cobalt molybdate with a magnifying force of 1 $\mu$ m, and 2 $\mu$ m; respectively. It seemed that cobalt molybdate oxide was prepared in the form of irregularly shaped nanoparticles and with various small and large sizes as seen in figure 4 b1 and b2.

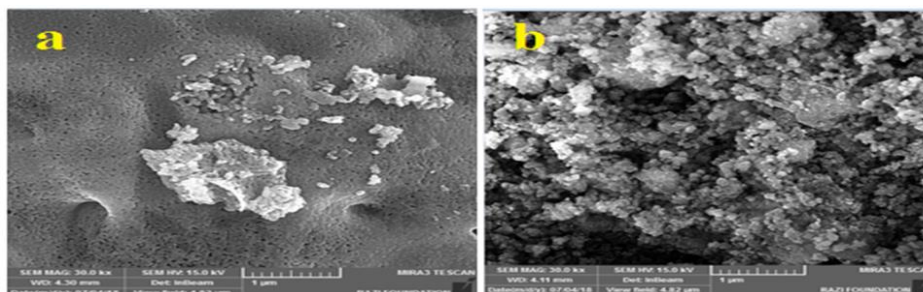


Figure 7. SEM of (a) G and (b) CoMoO<sub>4</sub>.

**3.1.4.3. SEM of cobalt molybdate- graphene:**

The scanning electron microscopy of the CoMoO<sub>4</sub>-G nanocomposite has been shown in figure 8 with magnification strength of 500 nm and 2 $\mu$ m; respectively, that in which there

was the distribution of CoMoO<sub>4</sub> nanoparticles on the surface of G sheets, and this was fully consistent with atomic force microscopy (AFM) results.

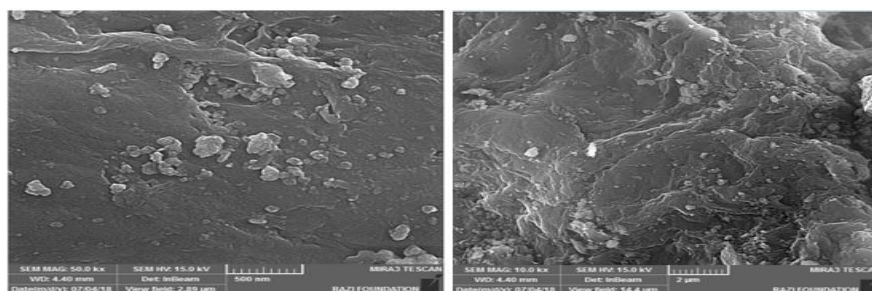


Figure 8. The scanning electron microscopy of the CoMoO<sub>4</sub>-G nanocomposite

### 3.2. Oxidative desulfurization of kerosene:

#### 3.2.1. Effect of loading percentage:

Different loading percentages (5%,10% and 15%) were examined to determine the optimum quantity of catalyst required for the oxidation reaction. The sulfur removal efficiency was increased by increasing the loading percent and reaching the maximum value of 62.5% when the loading of the nanoparticle on the graphene sheet was 15%, as shown in figure 9.

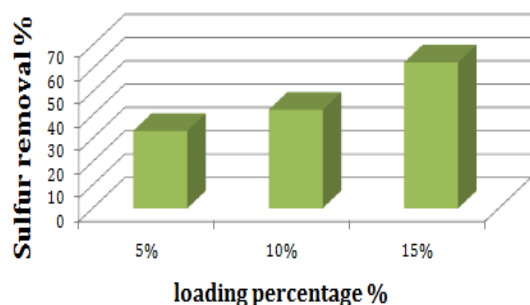


Figure 9. Effect of loading percentage on efficiency of total sulfur removal

#### 3.2.2. Effect of contact time:

Figure 10, shows the sulfur removal at time of 0.25-2 hour for the catalytic DBT oxidative desulfurization. There was no significant sulfur removal observed after 0.75 hour contact time. It was also noted that at the prolonged contact time of more than 1.5 hour, there was no much influence of time on the percentage of desulfurization due to the degradation of most H<sub>2</sub>O<sub>2</sub> oxidant.

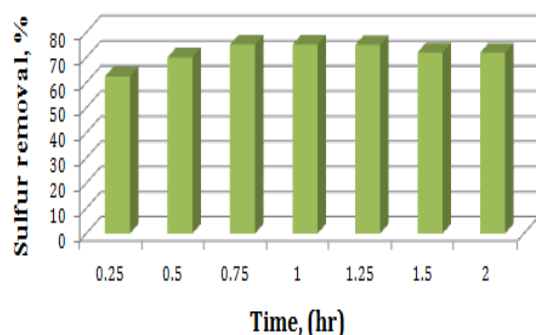


Figure 10. Sulfur removal at time of 0.25-2 hour for the catalytic DBT oxidative desulfurization

#### 3.2.3. Effect of reaction temperature:

The reaction temperature range of 35-80 °C was studied, and has been shown in Figure 11. The increase of reaction temperature from 30 to 60 °C increased the removal efficiency of sulfur from the simulated oil till it reached 80.1 % at 60°C and 70°C. The highest selected temperature used was 60°C, because it had the highest removal of sulfur as the high temperature initiates decomposition of H<sub>2</sub>O<sub>2</sub>, then destroys the oxidation ability (Abdul-Kadhim et al., 2017; Parvin et al., 2012). The results indicated that increasing the temperature would increase the internal energy between the reacted compounds and enhance the rapid molecular movement, which would cause increasing the removal efficiency of sulfur.

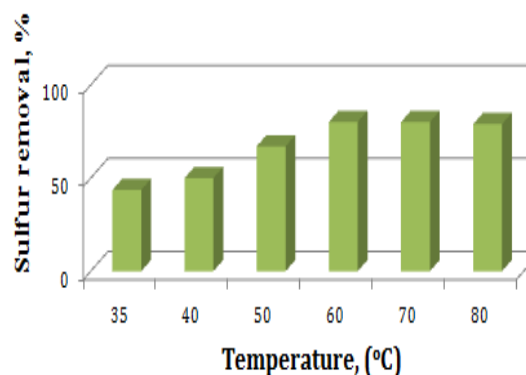


Figure 11. Effect of temperature on sulfur removal.

#### 3.2.4. Effect of O/S ratio:

The effect of the oxidizing agent (H<sub>2</sub>O<sub>2</sub>) to sulfur content ratio (O/S) on the desulfurization efficiency has been shown in Figure 12. The results showed that the sulfur removal efficiency was increased with increasing O/S ratio. When O/S equaled 5 molar ratios, which was higher than the reaction stoichiometry, the sulfur removal was 90 %. When O/S molar ratio increased to more than 5, the oxidant content resulted in decreasing the sulfur removal efficiency, due to the unproductive decomposition of H<sub>2</sub>O<sub>2</sub> to O<sub>2</sub> and water which reduced the oxidation efficiency.

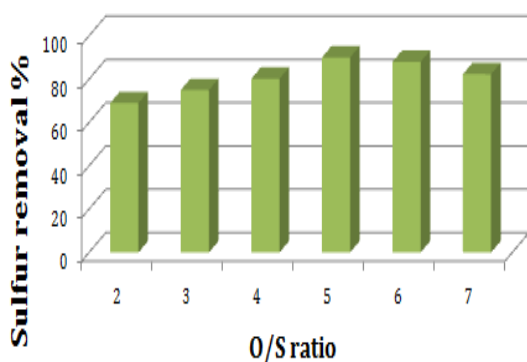


Figure 12. Effect of O/S molar ratio on sulfur removal.

### 3.2.5. Effect of catalyst weight:

Different catalyst masses of 0.1, 0.2, 0.3, 0.4, 0.5 and 0.6g were examined to determine the optimum quantity of catalyst for oxidation reaction as in Figure 13. The sulfur removal efficiency was increased by increasing the catalyst weight and reaching the maximum percentage removal of 93% when the weight of the catalyst was 0.4 g. The extra increase in the catalyst weight caused a decrease in the sulfur removal efficiency with less than 92.1 % at a catalyst weight of 0.5g. This decrease in efficiency could be attributed to an agglomeration and aggregation effects, which reduced the number of active sites on catalyst surface which then reduced the effective surface area available (Parvin et al., 2012).

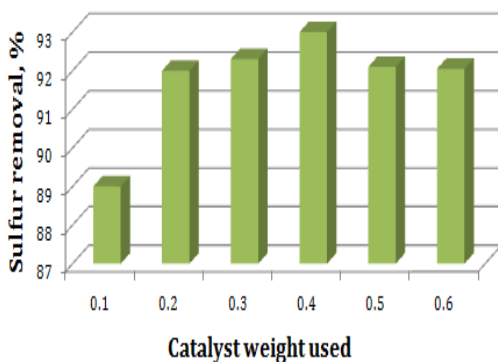


Figure 13. Effect of catalyst weight used on sulfur removal.

## 4. CONCLUSIONS:

CoMoO<sub>4</sub> samples were selected for the study of the removal of sulfur by oxidative desulfurization from kerosene, where the results showed that for the removal of sulfur (ODS), the higher loading rate (doping) of the reduced graphene oxides increased the rate of sulfur removal; where the highest percentage of removal of sulfur was with the loading rate of (15%).

In addition, different conditions were observed for the removal of sulfur (time, temperature, O / S ratio, catalytic mass), where the results showed that the increase in time and temperature

increased the removal of sulfur. The results also showed that by increasing the ratio of O / S, the mass of the catalyst increased the rate of the removal of sulfur until reaching a stable removal rate.

## REFERENCES

1. Abdul-Kadhim, W., Deraman, M. A., Abdullah, S. B., Tajuddin, S. N., Yusoff, M. M., Taufiq-Yap, Y. H., & Rahim, M. H. A. (2017). Efficient and reusable iron-zinc oxide catalyst for oxidative desulfurization of model fuel. *Journal of environmental chemical engineering*, 5(2), 1645-1656.
2. Babich, I. V., & Moulijn, J. A. (2003). Science and technology of novel processes for deep desulfurization of oil refinery streams: a review☆. *Fuel*, 82(6), 607-631.
3. Bösmann, A., Datsevich, L., Jess, A., Lauter, A., Schmitz, C., & Wasserscheid, P. (2001). Deep desulfurization of diesel fuel by extraction with ionic liquids. *Chemical Communications*, (23), 2494-2495.
4. Breyse, M., Djega-Mariadassou, G., Pessayre, S., Geantet, C., Vrinat, M., Pérot, G., & Lemaire, M. (2003). Deep desulfurization: reactions, catalysts and technological challenges. *Catalysis Today*, 84(3-4), 129-138.
5. De Filippis, P., & Scarsella, M. (2003). Oxidative desulfurization: oxidation reactivity of sulfur compounds in different organic matrixes. *Energy & Fuels*, 17(6), 1452-1455.
6. Deshpande, A., Bassi, A., & Prakash, A. (2005). Ultrasound-assisted, base-catalyzed oxidation of 4, 6-dimethyldibenzothiophene in a biphasic diesel-acetonitrile system. *Energy & Fuels*, 19(1), 28-34.
7. Gui, J., Liu, D., Sun, Z., Liu, D., Min, D., Song, B., & Peng, X. (2010). Deep oxidative desulfurization with task-specific ionic liquids: an experimental and computational study. *Journal of Molecular Catalysis A: Chemical*, 331(1-2), 64-70.
8. Hulea, V., Fajula, F., & Bousquet, J. (2001). Mild oxidation with H<sub>2</sub>O<sub>2</sub> over Ti-containing molecular sieves—a very efficient method for removing aromatic sulfur compounds from fuels. *Journal of catalysis*, 198(2), 179-186.
9. Kabe, T., Ishihara, A., & Tajima, H. (1992). Hydrodesulfurization of sulfur-containing polyaromatic compounds in light oil. *Industrial & engineering chemistry research*, 31(6), 1577-1580.
10. Kianpour, G., Salavati-Niasari, M., & Emadi, H. (2013). Precipitation synthesis and characterization of cobalt molybdates nanostructures. *Superlattices and Microstructures*, 58, 120-129.
11. Kumar, P., Gill, K., Kumar, S., Ganguly, S. K., & Jain, S. L. (2015). Magnetic Fe<sub>3</sub>O<sub>4</sub>@ MgAl-LDH composite grafted with cobalt phthalocyanine as an efficient heterogeneous catalyst for the oxidation of mercaptans. *Journal of Molecular Catalysis A: Chemical*, 401, 48-54.
12. Lei, W., Wenya, W., Mominou, N., Liu, L., & Li, S. (2016). Ultra-deep desulfurization of gasoline through

- aqueous phase in-situ hydrogenation and photocatalytic oxidation. *Applied Catalysis B: Environmental*, 193, 180-188.
13. Ma, X., Sakanishi, K., & Mochida, I. (1994). Hydrodesulfurization reactivities of various sulfur compounds in diesel fuel. *Industrial & engineering chemistry research*, 33(2), 218-222.
  14. Mokhtar, W. N. A. W., Bakar, W. A. W. A., Ali, R., & Kadir, A. A. A. (2015). Optimization of oxidative desulfurization of Malaysian Euro II diesel fuel utilizing tert-butyl hydroperoxide–dimethylformamide system. *Fuel*, 161, 26-33.
  15. Nakamoto K. (1997). *Infrared and Raman spectra of inorganic and coordination compounds*. New York: Wiley; 5th ed.
  16. Otsuki, S., Nonaka, T., Takashima, N., Qian, W., Ishihara, A., Imai, T., & Kabe, T. (2000). Oxidative desulfurization of light gas oil and vacuum gas oil by oxidation and solvent extraction. *Energy & fuels*, 14(6), 1232-1239.
  17. Parvin, T., Keerthiraj, N., Ibrahim, I. A., Phanichphant, S., & Byrappa, K. (2012). Photocatalytic degradation of municipal wastewater and brilliant blue dye using hydrothermally synthesized surface-modified silver-doped ZnO designer particles. *International Journal of Photoenergy*, 2012..
  18. Rudge, A., Davey, J., Raistrick, I., Gottesfeld, S., & Ferraris, J. P. (1994). Conducting polymers as active materials in electrochemical capacitors. *Journal of Power Sources*, 47(1-2), 89-107.
  19. Sieber, K., Kershaw, R., Dwight, K., & Wold, A. (1983). Dependence of Magnetic Properties on Structure in the Systems NiMoO<sub>4</sub> and CoMoO<sub>4</sub>. *Inorg. Chem.* 22(19), 2667–2669.
  20. Silverstein R. M., (1962). "Spectroscopic identification of organic compounds", 6th ed, F. X Webster.
  21. Te, M., Fairbridge, C., & Ring, Z. (2001). Oxidation reactivities of dibenzothiophenes in polyoxometalate/H<sub>2</sub>O<sub>2</sub> and formic acid/H<sub>2</sub>O<sub>2</sub> systems. *Applied Catalysis A: General*, 219(1-2), 267-280.
  22. Triantafyllidis, K. S., & Deliyanni, E. A. (2014). Desulfurization of diesel fuels: adsorption of 4, 6-DMDBT on different origin and surface chemistry nanoporous activated carbons. *Chemical Engineering Journal*, 236, 406-414.
  23. William, S., Hummers, J. R., & Offeman, R. E. (1958). Preparation of graphitic oxide. *J. Am. Chem. Soc.* 80(6), 1339-1339.
  24. Yazu, K., Yamamoto, Y., Furuya, T., Miki, K., & Ukegawa, K. (2001). Oxidation of dibenzothiophenes in an organic biphasic system and its application to oxidative desulfurization of light oil. *Energy & Fuels*, 15(6), 1535-1536.
  25. Zhao, D., Ren, H., Wang, J., Yang, Y., & Zhao, Y. (2007). Kinetics and mechanism of quaternary ammonium salts as phase-transfer catalysts in the liquid– liquid phase for oxidation of thiophene. *Energy & Fuels*, 21(5), 2543-2547.